Icarus 394 (2023) 115403

Contents lists available at ScienceDirect

Icarus

journal homepage: www.elsevier.com/locate/icarus

An observing campaign to search for meteoroids of Bennu at Earth

Peter Jenniskens [a,b,*], Dante S. Lauretta [c], Lindsey R. Koelbel [c], Martin C. Towner [d], Phil Bland [d], Steve Heathcote [e], Timothy M.C. Abbott [e], Emmanuel Jehin [f], Toni Hanke [g], Elise Fahl [g], Rynault van Wyk [g], Tim Cooper [h], Jack W. Baggaley [i], Dave Samuels [a], Peter S. Gural [j]

[a] SETI Institute, 339 Bernardo Ave, Mountain View, CA 94043, USA
[b] NASA Ames Research Center, Moffett Field, CA 94035, USA
[c] Lunar and Planetary Laboratory, University of Arizona, Tucson, AZ 85721, USA
[d] Space Science and Technology Centre, Curtin University, Perth, WA 6102, Australia
[e] Cerro Tololo Inter-American Observatory, NSF's National Optical-Infrared Astronomy Research Laboratory, Casilla 603, La Serena, Chile
[f] STAR Institute, University of Liège, B-4000 Liège 1, Belgium
[g] High Energy Stereoscopic System Experiment, Windhoek 11009, Namibia
[h] Astronomical Society of Southern Africa, Bredell 1623, Kempton Park, South Africa
[i] University of Canterbury, Christchurch 8041, New Zealand
[j] Gural Software and Analysis LLC, Lovettsville, VA 20180, USA

ARTICLE INFO

Keywords:
Meteors
Asteroid Bennu
Zodiacal light

ABSTRACT

An observing campaign was conducted in the Southern Hemisphere using low-light video camera triangulation to measure the trajectories and orbits of meteoroids with a possible origin at asteroid Bennu. New CAMS (Camera for Allsky Meteor Surveillance) video camera networks were established in Australia, Chile, and Namibia, and networks in New Zealand and South Africa were expanded. During observing periods in September 2019, 2020, and 2021, we measured 7672, 4936, and 5890 orbits, respectively. Based on the non-detection of predicted meteoroid trail encounters, Bennu's meteoroid production rate was <1.5 kg/s during 1500–1800 CE. Indeed, the current production rate is many orders of magnitude lower. Bennu may have an associated annual meteoroid stream of much older ejecta at a particle flux density of $\leq 1.3 \times 10^{-6}$ km^{-2} h^{-1}, based on seven Bennu-like orbits detected during the first three years of observations.

1. Introduction

During orbital observations at asteroid (101955) Bennu, NASA's OSIRIS-REx mission team discovered that the asteroid was episodically emitting millimeter- to centimeter-sized particles, about 30% of which escaped Bennu on hyperbolic trajectories (Lauretta et al., 2019; Hergenrother et al., 2020; Chesley et al., 2020). The ejection mechanism and the epoch of activity remain unknown.

Asteroid Bennu moves in an almost Earth-like orbit around the Sun, passing only 0.0030 AU from Earth's orbit itself at the current epoch. The JPL#118 solution orbit of Bennu (cneos.jpl.nasa.gov, for the epoch of 2011-Jan-01.0 TDB) has a low eccentricity (e = 0.204), a semi-major axis close to 1 AU (a = 1.13 AU), and low inclination ($i = 6.03°$).

The heliocentric orbit of the ejected particles will evolve over time due to gravitational perturbations and radiation forces, possibly into orbits that can put them on a collision course with Earth. Ye (2019) first studied the dynamical evolution of ejecta and calculated the expected meteoroid flux density at Earth, assuming cometary style production and, using the then current upper limit to the meteoroid production rate of 0.15 kg/s. He concluded that rates would stay below zenith hourly rate ZHR = 1 per hour in the coming years (equivalent to a meteoroid flux density of ~10^{-6} km^{-2} h^{-1}), but also predicted higher rates in the 2090's when Bennu's orbit would come closer to Earth, and encouraged monitoring now to possibly detect unusual activity of Bennu in the past. Meteors would enter Earth's atmosphere with a low apparent entry speed of $V_\infty = 12.7$ km s^{-1} in late September.

The predictions by Ye (2019) were updated by Kovácová et al. (2020), who studied the dynamical evolution of a cloud of 5000 particles ejected gradually in the year 1600 CE, providing insight into the stream dispersion. A meteor shower at Earth was predicted to have a relatively compact radiant with dispersions at geocentric coordinates $R.A._g = 3.3 \pm 2.1°$ and $Decl._g = -34.7 \pm 1.7°$.

* Corresponding author at: SETI Institute, 339 Bernardo Ave, Mountain View, CA 94043, USA.
E-mail address: pjenniskens@seti.org (P. Jenniskens).

https://doi.org/10.1016/j.icarus.2022.115403
Received 25 October 2022; Received in revised form 12 December 2022; Accepted 14 December 2022
Available online 16 December 2022

More recent estimates of flux density by Melikyan et al. (2021) put the anticipated rates orders of magnitude lower. Melikyan et al. integrated 1.8 million particles during the years 1780–2135 when the orbit of Bennu is precisely known, and took into account that, unlike cometary ejection, particles are produced along the entire orbit of the asteroid (Hergenrother et al., 2020). They found impacts at Earth only starting in 2101, with highest rates later that century, and especially in the year 2182. Hergenrother et al. estimated the particle production rate on average at only ~2.5 kg/y, ejection speeds between 0.2 and 3.3 m/s. Chesley et al. (2020) estimated particle densities of order 2.0 g/cm^3 and particle sizes in the range 0.1–7 cm.

Based on the earlier more optimistic shower flux densities at Earth, an effort was made to search for meteoroids with an origin at Bennu. The asteroid orbit passes close enough to Earth's orbit to anticipate both dispersed annual stream activity as well as potential outbursts from relatively recent ejecta. Centimeter-sized meteoroids entering Earth's atmosphere with an apparent initial speed $V_\infty = 12.7$ km s^{-1} would produce meteors of visual magnitude +0.2 (Jacchia et al., 1967; Jenniskens, 2006). Hence, the size of the meteoroids and their expected slow impact speed call for low-light video observations, rather than radar observations that would detect smaller grains, or photographic all-sky observations that would detect much larger grains. Moreover, at the low speeds of Bennu meteoroids, the ionization efficiency drops by several orders of magnitude, making detection of such slow meteoroids by radar inefficient (Brown and Weryk, 2020).

To search for potential meteor shower activity from asteroid Bennu, three CAMS (Cameras for Allsky Meteor Surveillance) low-light video camera networks (Jenniskens et al., 2011) were built and deployed in the Southern Hemisphere in Australia, Chile and Namibia in 2019. An existing network in New Zealand was expanded and a small network was established in South Africa. This geographic spread of networks optimized the chance of having clear weather in the relevant time period in at least one of the networks. Also, it enabled monitoring of variable shower activity and meteor outbursts on short hourly timescales from meteoroid streams that have not yet dispersed widely. The networks were in place before late August 2019, so that Bennu's expected stream could be observed first in late September of that year. Once established, the networks continued monitoring the Bennu stream annually, to maximize the number of meteoroids detected and to detect annual variations in activity.

In the years since, these new Southern Hemisphere CAMS video camera networks have provided much new insight into other meteor showers. This included a predicted detection of debris from comet 15P/Finlay, causing a shower now called the Arids, which had encounter conditions with Earth not unlike those for the debris of Bennu (Jenniskens, 2021a, 2021b). One of the first discoveries reported was a meteor shower associated with comet C/1939 H_1 (Jenniskens et al., 2019). Since that initial discovery, other long-period comet showers were found (Jenniskens et al., 2021); these observations revealed that all known comets with orbital periods <4000 years passing within 0.10 AU of Earth's orbit have detectable meteor showers.

Here, we report on the results pertaining to the search for a possible meteor shower from asteroid Bennu. We did not detect with certainty meteors that originated from Bennu, but did find some meteors in orbits similar to that of Bennu.

Fig. 1. Newly established camera network CAMS Australia: A) station at Curtin University, B) in Red Gully, and C) in Bindoon; CAMS Chile: D) station at Cerro Tololo observatory, E) at La Silla observatory, F) in La Serena; and CAMS Namibia: G) station at the H.E.S.S. telescopes, H) in Windhoek, and I) in Rehoboth.

2. Methods

Each new CAMS network contained three individual camera stations that operated 16 cameras in a fly's eye configuration covering the sky above 30° elevation. The stations were deployed at three sites near Perth, Western Australia, at three sites near La Serena, Chile, and at three sites near Windhoek, Namibia (Fig. 1). Research teams at Curtin University (Australia), Association of Universities for Research in Astronomy AURA/Cerro Tololo (Chile), and the High Energy Stereoscopic System (H.E.S.S.) Collaboration (Namibia) agreed to manage and maintain the camera stations.

Each CAMS station consisted of a PC, 16 Watec Wat902 H2 Ultimate cameras, 13 Ricoh model C61215KP f1.2 12-mm lenses and 3 Spacecom JF8M-2 f1.3 18-mm lenses, 2 CCTV power supplies, 2 Sensoray model 812 frame grabbers, a camera enclosure with an anti-reflection coated flat optical window, camera stands, a heating element, and three timers (Jenniskens et al., 2011).

The camera mounts and environmental boxes to house the cameras were built suitable for deployment abroad. The PC software, frame grabber cards, cameras, and environmental housing were tested, and the lenses were focused. The stations were set up in each country and equipment was tested in the field, resulting in nine new CAMS stations. In addition, we upgraded the CAMS New Zealand network with an additional station in Ashburton and established a small 16-camera network near Johannesburg in South Africa (CAMS South Africa).

Daily meteor radiant and velocity data were presented in near-real time at http://cams.seti.org/FDL/, and can still be accessed for the past dates. For a period of time around the expected occurrence of the shower, all automatically reduced triangulations reported at this daily website were subsequently reduced again manually, and each solution verified by making sure the astrometry from each station aligned in trajectory and light curve, as required. From this, an orbit database was created for the September 2019, 2020, and 2021 observing seasons, together with information about the camera performances and weather.

3. Results

We derived 7672 orbits in 2019 (September 18–29), 4936 in 2020 (September 19–28), and 5890 in 2021 (September 16–30). Weather (clouds, haze) affected the observations in various amounts. Table 1 summarizes the reduction in network efficiency of detection compared to the case where all cameras are working and the sky is clear. For example, all networks suffered from bad weather on some days in 2021, but with a single exception got results on every night during the observing period. CAMS Australia detected many insects, which slowed the data reduction effort, but did not result in lost meteors based on the yield compared to other networks.

Fig. 2 shows the radiant positions of observed meteors in the combined 2019–2021 data, divided into two regimes — asteroidal (left) and cometary (right) meteors — as measured by each orbit's Tisserand Parameter with respect to Jupiter (T_J), with the semi-major axis for Jupiter taken as $a_J = 0.520336$ AU, and the semi-major axis (a), inclination (i) and eccentricity (e) of the meteoroid orbit:

$$T_J = a_J/a + 2\,cos(i)\sqrt{[a/a_J\,(1-e^2)\,]} \quad (1)$$

Radiant positions are expressed in Sun-centered ecliptic longitude and latitude, which corrects the geocentric radiant coordinates for the daily radiant drift from Earth's motion around the Sun.

The left asteroidal ($T_J > 3$) diagram shows no cluster of meteor radiants at the theoretical radiant position (crosses), but there is a diffuse scattering of radiants surrounding the theoretical radiant position, and some of those meteoroids moved in orbits similar to that of Bennu. The Southworth and Hawkins (1963) D-criterion (D_{SH}) in the approximation of having small inclinations was used to identify such orbits, with meteoroid orbit and Bennu's orbit given, respectively, by eccentricity e_1 and e_2, perihelion distance q_1 and q_2, inclination i_1 and i_2, node Ω_1 and Ω_2, and longitude of perihelion Π_1 and Π_2:

$$D^2 = [e_2 - e_1]^2 + [q_2 - q_1]^2 + [2\sin((i_2 - i_1)/2)\,]^2 \quad (2)$$

$$[D_{SH}]^2 = D^2 + sin(i_1)sin(i_2)[2sin((\Omega_2 - \Omega_1)/2)]^2 + [e_1 + e_2]^2[sin((\Pi_2 - \Pi_1)/2)]^2 \quad (3)$$

Seven meteors have $D_{SH} < 0.1$ (Table 2), a reasonable limit for stream association for Jupiter-family type orbits (Lindblad, 1971; Moorhead, 2016). One of these has a radiant position relatively far from the theoretical position. In Table 2, the orbital elements are compared to those of Bennu after adjusting its orbit to intersect that of Earth according to method Q of Neslusan et al. (1998).

The right cometary ($T_J \leq 3$) diagram has only one radiant at exactly the calculated theoretical position for Bennu's meteor shower, but that radiant position has a relatively large observational uncertainty, and the measured velocity is 2σ off (first entry marked "*" in Table 2). The second meteor marked by "*" has small formal uncertainties in radiant position and speed. Both solutions have inclination off by ~2°, node off by 1.8°, and eccentricity off by 0.07. If these meteoroids are from Bennu, then these differences reflect some perturbations since ejection.

Fig. 3 shows the eccentricity of orbits in the cloud around the theoretical radiant position of Bennu. The group of six orbits with $e \sim 0.2$ stands out from the rest of the sporadic population (Table 4). One orbit listed in Table 4 has a radiant outside this group. The D-criterion selects meteors over a large range of ecliptic latitude of the radiant.

Did weather conditions allow for the relevant interval in solar longitude to be covered by the observations? Ye (2019) predicted an encounter with meteoroids from 1523 to 1791 CE around 2019 September 25 at 12:26 UTC (corresponding to solar longitude 181.880°), and from the 1507–1682 CE ejecta around 2021 September 24 at 21:16 UTC (corresponding to solar longitude 181.741°), and each encounter would be about 10 h wide.

Indeed, the weather was clear in those time intervals. In 2019 176 meteors were detected by CAMS Chile, CAMS New Zealand, and CAMS Australia in the relevant time interval between solar longitude 181.676 and 182.084° (September 25 7:26–17:26 UTC). None were within 10° from the theoretical radiant position. In 2021, 132 meteors were detected again by CAMS Chile, CAMS New Zealand, and CAMS Australia in the relevant time interval between solar longitude 181.057 and 181.465° (September 24 16:16 – September 25 2:16 UTC). This time, two meteors were detected very close to the theoretical radiant position, but both had a high $V_g \sim 20$ km s^{-1} entry speed, resulting in the Jupiter-family comet type orbits listed in Table 3.

Table 1
The effect of weather and technical performance on the daily yield of meteor orbits during the three September Bennu observing campaigns in 2019–2021.

Network:		#Cam:	Fraction of time clear and operating:			T_{eff}:	Yield:
#	Site:		2019	2020	2021	(h)	(per day)
15	Australia	48	0.62	0.37	0.30	10.5	292
16	Chile	48	0.93	0.40	0.27	10.6	278
17	Namibia	48	0.80	0.86	0.43	10.7	290
5	New Zealand	48	0.53	0.56	0.55	10.0	151*
8	South Africa	16	0.69	0.53	0.27	10.5	72

Notes: T_{eff} is the effective observing time. *) One of the stations is at a large distance from the other two.

4. Discussion

4.1. Radiant dispersion and shower duration

It is often stated that the meteor shower radiant distribution is more diffuse when the encounter speed is low, because the Earth's gravity and

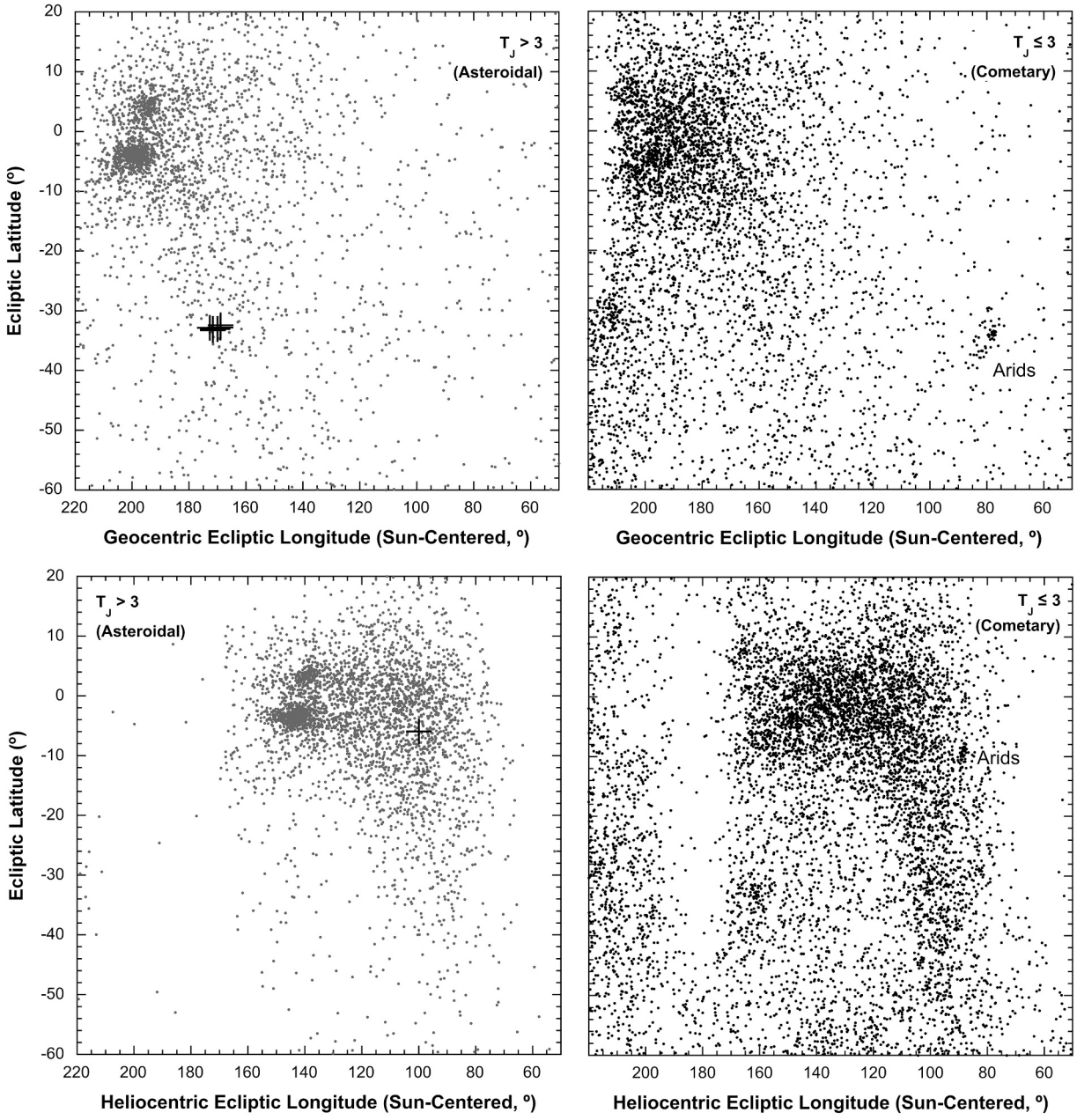

Fig. 2. Radiant maps of combined data for the 2019–2021 seasons, divided into two regimes of the Tisserand Parameter with respect to Jupiter and plotted in geocentric (top) and heliocentric (bottom) ecliptic coordinates. Zero longitude marks the position of the Sun, zero latitude the position of the ecliptic plane. At the top of each figure, centered on the ecliptic plane, is the anthelion source, containing early Northern and Southern Taurids on short asteroidal orbits. The crosses mark theoretical radiants for Bennu meteoroids according to approaches used by Neslusan et al. (1998), with the heliocentric plot only showing the "Q" method for clarity.

Table 2
Time of appearance, radiant, speed, and orbital elements of the detected meteoroids that are in orbits most similar to the current JPL#118 solution orbit of Bennu (lowest row, corrected for bridging the miss-distance to Earth).

Sol. Long.	R.A.$_g$	Decl.$_g$	V$_g$	q	e	i	ω	Ω	D_{SH}	Yr
(°)	(°)	(°)	(km s^{-1})	(AU)		(°)	(°)	(°)		
175.345	14.3 ± 2.3	−43.7 ± 0.8	8.23 ± 0.18	0.870	0.227	10.9	74.1	355.3	0.094	2021
180.995	2.6 ± 1.0	−38.6 ± 0.9	6.95 ± 0.12	0.907	0.245	7.4	59.2	1.0	0.058	2020
*183.913	6.5 ± 0.2	−36.2 ± 0.4	7.64 ± 0.04	0.894	0.266	8.0	61.1	3.9	0.073	2019
183.886	355.0 ± 1.2	−11.1 ± 3.8	4.94 ± 0.46	0.899	0.197	1.3	68.0	3.9	0.084	2019
*183.354	5.0 ± 5.2	−29.7 ± 5.8	3.75 ± 0.62	0.924	0.136	3.4	69.8	3.4	0.088	2019
184.141	8.6 ± 3.3	−40.7 ± 3.8	7.11 ± 0.48	0.910	0.239	8.3	58.7	4.2	0.059	2019
185.271	9.1 ± 0.4	−21.4 ± 4.1	6.84 ± 0.41	0.849	0.238	5.1	78.1	5.3	0.084	2020
182.062	*5.5*	*−34.3*	*5.93*	*0.902*	*0.204*	*6.0*	*66.2*	*2.1*	*Bennu*	*Q*

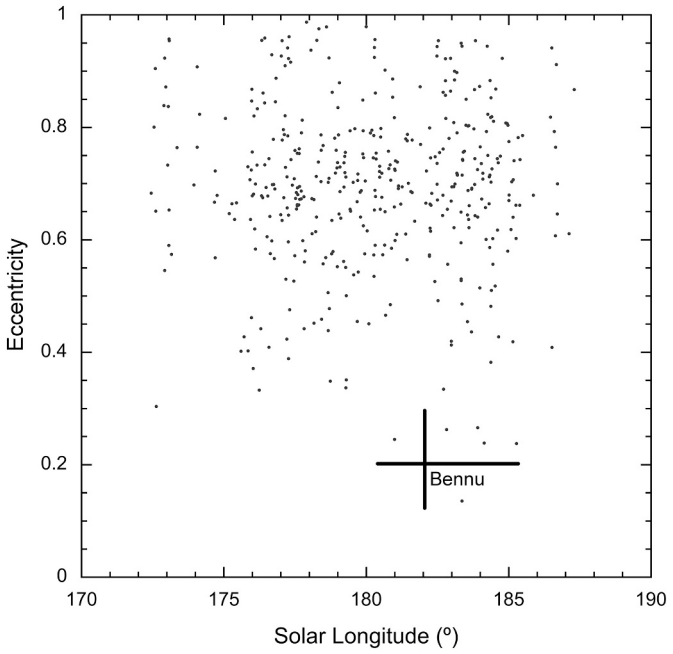

Fig. 3. The eccentricity of measured orbits in the diffuse region of radiants surrounding the theoretical radiant position from Bennu.

spin tend to change the direction of motion of the meteoroids by moving the radiant to the zenith and broadening the radiant dispersion. That would make slow meteor showers more difficult to separate from the sporadic meteor background.

On the other hand, those effects are removed from the orbits by converting apparent radiant and speed into geocentric radiant and speed (Gural, 2000). This was verified in observations of the Arids, an irregular meteor shower that originates from comet 15P/Finlay and was detected during the Bennu observing season in 2021 (Fig. 2). Based on model calculations by Maslov (2009) and Vaubaillon et al. (2020), dust trails from the 1988 and the 1995 return of 15P/Finlay were crossed in 2021. Each produced a ~ 10-h-duration shower with a different radiant position due to the gravitational perturbations on the comet orbit itself (Table 4). The observed radiant positions are in excellent agreement with the theoretical radiant positions, confirming the accuracy of the correction to geocentric radiant positions (Gural, 2000).

The Arid meteors entered at a low speed of $V_\infty = 15.7$ km s^{-1} (1988 dust trail) and 15.4 km s^{-1} (1995 dust trail), respectively, only slightly faster than the anticipated Bennu meteors. The observed radiants are compact and stand out well from the sporadic background. For the Bennu showers, the gravitational attraction of Earth is expected to disperse the stream somewhat wider, but we would still expect to find a compact geocentric radiant for meteoroids that move in similar orbits after correction for the effects of Earth's gravity. Only if the planetary perturbations spread the material further would a more diffuse radiant result.

A further concentration of shower radiants was shown to occur for slow meteors in the heliocentric ecliptic coordinate frame (Tsuchiya et al., 2017). Heliocentric ecliptic coordinates of the radiant position are routinely provided by CAMS and are shown in the two bottom graphs of Fig. 2. Again, we do not see a concentration of radiants around the theoretical position (marked by a cross) like that of the Arids.

4.2. Sensitivity limit

How sensitive was the network for detecting the Bennu meteoroid flux? Cometary meteoroids entering at 12.7 km s^{-1} have a beginning altitude of about 88 km and an end altitude of 80 km on average, while asteroidal meteoroids have a beginning altitude of 78 km and end altitude of 70 km. For an altitude of 80 km, the effective surface area of each network (where bright meteors are detected) is an about circular area with a diameter of ~342 km. That gives an effective surface area of ~92,000 km^2.

Bright meteors are more efficiently triangulated than faint meteors due to distance losses in apparent brightness. Table 5 gives the brightness-dependent detection efficiency of the southern hemisphere CAMS networks for an entry speed of ~15 km s^{-1}. This function was derived from the observed Arid meteor magnitude distribution, assuming it had an exponential distribution also in the magnitude regime where not all meteors provided orbits. Based on similar data from showers with other entry velocities, these numbers should be close to those for the Bennu meteors at about 12.7 km s^{-1}. A fraction of 85–100% of +0.2-magnitude meteors are detected over the full survey area.

The effective observing time for slow meteors — the total observing time through the night (not taking into account the radiant elevation dilution) — is given in Table 1. If the flux of +0.2-magnitude Bennu meteors is constant, then the detection efficiency for one main network during a 10.5-h night is about 2×10^{-6} km^{-2} h^{-1} in a given night, after

Table 3
As Table 2, for two 2021 meteoroids with radiants close to the theoretical radiant position and time of a Bennu shower, but having deviating entry speed.

Sol. Long. (°)	R.A.$_g$ (°)	Decl.$_g$ (°)	V_g (km s^{-1})	q (AU)	e	i (°)	ω (°)	Ω (°)	D_{SH}	Yr
181.262	3.0 ± 0.3	−32.8 ± 0.3	18.02 ± 0.09	0.794	0.694	15.6	60.6	1.3	0.531	2021
181.386	6.4 ± 0.7	−33.5 ± 0.8	20.69 ± 0.81	0.769	0.780	18.9	62.2	1.4	0.632	2021
182.062	*5.5*	*−34.3*	*5.93*	*0.902*	*0.204*	*6.0*	*66.2*	*2.1*	*Bennu*	*Q*

Table 4
Arid shower median radiant positions in 2021, in predictions and as observed (Obs:).

Encounter 2021 (UTC)	Eject (Yr)	λ_o (°)	R.A.$_g$ (°)	Decl.$_g$ (°)	V_g (km s^{-1})	ZHR (h^{-1})	χ	
09/27 06:14	1988	184.067	264.1	−60.5	11.0	-.-	-.-	[1]
09/27 13:58–16:22	"	184.432	261.1	−60.5	11.0	5–100	2.5	[2]
Obs:	"	*184.35 ± 0.18*	*261.6 ± 0.7*	*−60.9 ± 0.4*	*11.2 ± 0.4*	*N = 12*	*2.52 ± 0.20*	
09/28 18:58	1995	185.569	261.6	−57.7	10.82	-.-	-.-	[1]
09/29 02:30–04:17	"	185.914	261.6	−57.7	10.8	50–500	2.5	[2]
09/29 08:35	"	186.072	260.8 ± 0.9	−57.4 ± 0.5	10.807	13	2.5	[3]
Obs:	"	*186.10 ± 0.07*	*261.0 ± 1.0*	*−57.3 ± 0.3*	*10.5 ± 0.2*	*N = 38*	*2.28 ± 0.11*	

Notes: [1] Jenniskens (2006); [2] Maslov (2009); [3] Vaubaillon et al. (2020).

Table 5
Estimated fraction of meteors observed by the southern hemisphere CAMS networks as a function of the magnitude of meteors with apparent entry speed of ~15 km s^{-1}.

magnitude:	≤ − 1	0	+1	+2	+3	+4	+5	+6
P(m)	1.00	1.00	0.75	0.44	0.17	0.024	0.0003	0.0

including a factor of 2 accounting for observing efficiency reduction due to bad weather (Table 1).

The predicted Bennu fluxes from recent ejecta in 2019 and 2021 in estimates by Ye (2019) were only of order $(1 \times 10^{-7}) - (2 \times 10^{-7})$ km^{-2} h^{-1}. These values are too low by an order of magnitude to be detected. The three main networks together, each observing for a 10-day period per year for three years, would detect one Bennu meteoroid if the mean flux is about 2×10^{-7} km^{-2} h^{-1}. If the seven detected low-eccentricity meteors are from Bennu (Table 2), then the annual shower has a mean flux of about 1.3×10^{-6} km^{-2} h^{-1}.

Given the now more reliable estimates of the present asteroid's particle production rate of $\sim 8 \times 10^{-8}$ kg/s by Hergenrother et al. (2020) and Melikyan et al. (2021), the past activity of Bennu would need to have been 7 orders of magnitude higher to have been detected by the current video camera network, with Ye's initial estimate of 0.15 kg/s providing a 1.5 kg/s upper limit to the asteroid's particle production rate during 1500–1800 CE.

5. Conclusions

The detection of slow Arids from 15P/Finlay during the 2021 observing season confirms that recently ejected Bennu meteoroids would have produced a compact radiant near the theoretical radiant position. No compact shower from Bennu's meteoroids was detected in the first three years of observations in 2019–2021. Two meteors detected at the right time and at the right radiant position in the 2021 observing season both have an entry speed too high to have originated from Bennu. Based on the current particle production rates of Bennu, this result is in line with expectations.

Bennu may have an associated annual meteoroid stream of much older ejecta at a particle density of $\leq 1.3 \times 10^{-6}$ km^{-2} h^{-1}, based on seven Bennu-like orbits detected during three years of observations. This population, however, can also have originated from other sources.

A successful detection of Bennu meteoroids in the future may not be expected until well into the next century and then will require an expansion of the current video triangulation capability in the Southern Hemisphere.

Declaration of Competing Interest

None.

Data availability

The manually reduced orbital elements derived during the 2019–2021 Bennu activity monitoring seasons are available from the corresponding author upon request.

Acknowledgements

We thank C. Wolner (LPL/University of Arizona) for an internal review of the paper. This material is based upon work supported by NASA under Contract NNM10AA11C issued through the New Frontiers Program.

References

Brown, P., Weryk, R.J., 2020. Coordinated optical and radar measurements of low velocity meteors. Icarus 352 id. 113975.
Chesley, S.R., French, A.S., Davis, A.B., Jacobson, R.A., Brozovic, M., Farnocchia, D., et al., 2020. Trajectory and estimation for particles observed in the vicinity of (101955) Bennu. JGR Planets 125 article id. e2019JE006363.
Gural, P., 2000. Fully correcting for the spread in meteor radiant positions due to gravitational attraction. JIMO 29, 134–138.
Hergenrother, C.W., Adam, C.D., Chesley, S.R., Lauretta, D.S., 2020. Introduction to the special issue: exploration of the activity of asteroid (101955) Bennu. JGR Planets 125 e2020JE006549.
Jacchia, L.G., Verniani, F., Briggs, R.E., 1967. An analysis of the atmospheric trajectories of 413 precisely reduced photographic meteors. Smiths. Contrib. Astrophys. 10, 1–139.
Jenniskens, P., 2006. Meteor Showers and their Parent Comets. Cambridge University Press, Cambridge, 790 pp.
Jenniskens, P., 2021a. In: Green, D.W.E. (Ed.), Arid Meteors 2021. CBET 5055 (2021 Oct. 09). CBAT, 1 pp.
Jenniskens, P., 2021b. In: Green, D.W.E. (Ed.), Arid Meteors 2021. CBET 5046 (2021 Oct. 01). CBAT, 1 pp.
Jenniskens, P., Gural, P.S., Dynneson, L., Grigsby, B.J., Newman, K.E., Borden, M., Koop, M., Holman, D., 2011. CAMS: Cameras for Allsky Meteor Surveillance to establish minor meteor showers. Icarus 216, 40–61.
Jenniskens, P., Lauretta, D.S., Towner, M.C., Bland, P.A., Heathcote, S., Jehin, E., Hanke, T., Cooper, T., Baggaley, J., 2019. First results from an observing campaign to detect the meteoroids of Bennu at Earth. In: Asteroid Science in the Age of Hayabusa 2 and OSIRIS-REx, held 5-7 Nov., 2019, in Tucson, AZ. LPI Contr. No. 2189, ed. 2017.
Jenniskens, P., Lauretta, D.S., Towner, M.O., Heathcote, S., Jehin, J., Hanke, T., Cooper, T., Baggaley, J.W., Howell, J.A., Johannink, C., Breukers, M., Odeh, M., Moskovitz, N., Juneau, L., Beck, T., De Cicco, M., Samuels, D., Rau, S., Albers, J., Gural, P.S., 2021. Meteor showers from known long period comets. Icarus 365 article id. 114469.
Kovácová, M., Nagy, R., Kornos, L., Tóth, J., 2020. 101955 Bennu and 162173 Ryugu: dynamical modelling of ejected particles to the Earth. Planet Space Sci. 185 article id. 104897.
Lauretta, D.S., Hergenrother, C.W., Chesley, S.R., Leonard, J.M., Pelgrift, J.Y., Adam, C. D., Al, Asad M., Antreasian, P.G., Ballouz, R.-L., Becker, K.J., Bennett, C.A., Bos, B.J., Bottke, W.F., Brozovic, M., Campins, H., Connolly Jr., H.C., Daly, M.G., Davis, A.B., de León, J., DellaGiustina, D.N., Drouet d'Aubigny, C.Y., Dworkin, J.P., Emery, J.P., Farnoccia, D., Glavin, D.P., Golish, D.R., Hartzell, C.M., Jacobson, R.A., Jawin, E.R., Jenniskens, P., Kidd, J.N., Lessac-Chenen, E.J., Li, Y.-Y., Libourel, G., Licandro, J., Lionis, A.J., Maleszeweksi, C.K., Manzoni, C., May, B., McCarthy, L., McMahon, J.W., Michel, P., Molaro, J.L., Nelson, D.S., Owen, J.W.M., Rizk, B., Roper, H.L., Rozitis, B., Sah, E.M., Scheeres, D.J., Seabrook, J.A., Selznick, S.H., Takahashi, Y., Thuillet, F., Tricarico, P., Vokrouhlicky, D., Wolner, C.W.V., 2019. OSIRIS-REx discovery of particle ejection from asteroid (101955) Bennu. Science 366, 3544–3546.
Lindblad, B.A., 1971. 2. A computerized stream search among 2401 photographic meteor orbits. Smiths. Contr. Astrophys. 12, 14–24.
Maslov, M., 2009. website: http://feraj.ru/Radiants/Predictions/1901-2100eng/Finlayids1901-2100predeng.html. Last accessed 2021 Sept 30.
Melikyan, R.E., Clark, B.E., Hergenrother, C.W., Chesley, S.R., Noaln, M.C., Ye, Q.-Z., Lauretta, D.S., 2021. Bennu's natural sample delivery mechanism: estimating the flux of Bennuid meteors at Earth. JGR Planets 126 article id. e2021JE006917.
Moorhead, A.V., 2016. Performance of D-criteria in isolating meteor showers from the sporadic background in an optical data set. Mon. Not. R. Astron. Soc. 455, 4329–4338.
Neslusan, L., Svoren, J., Proubcan, V., 1998. A computer program for calculation of a theoretical meteor-stream radiant. Astron. Astrophys. 331, 411–413.
Southworth, R.B., Hawkins, G.S., 1963. Statistics of meteor streams. Smiths. Contrib. Astrophys. 7, 261–285.
Tsuchiya, C., Sato, M., Watanabe, J.-I., Moorhead, A.V., Moser, D.E., Brown, P.G., Cooke, W.J., 2017. Planet Space Sci. 143, 142–146.
Vaubaillon, J., Egal, A., Desmars, J., Baillié, K., 2020. Meteor shower output caused by comet 15P/Finlay. JIMO 48, 29–35.
Ye, Q., 2019. Prediction of meteor activities from (101955) Bennu. Research Notes of the American Astronomical Society 3 article id. 56.